Theoretical study of transition-metal hydrides. 5. Hafnium to mercury (HfH+ through HgH+), barium and lanthanum (BaH+ and LaH+)

ARTICLE *in* JOURNAL OF THE AMERICAN CHEMICAL SOCIETY · SEPTEMBER 1990

Impact Factor: 12.11 · DOI: 10.1021/ja00176a016

3 AUTHORS, INCLUDING:

Gilles Ohanessian
French National Centre for Scientific Resea…
115 PUBLICATIONS **3,674** CITATIONS
SEE PROFILE

William A. Goddard
California Institute of Technology
1,330 PUBLICATIONS **67,356** CITATIONS
SEE PROFILE

Theoretical Study of Transition-Metal Hydrides. 5. HfH^+ through HgH^+, BaH^+, and LaH^+

Gilles Ohanessian,† Mark J. Brusich,‡ and William A. Goddard III*

Contribution No. 8073 from the Arthur Amos Noyes Laboratory of Chemical Physics, California Institute of Technology, Pasadena, California 91125. *Received December 6, 1989*

Abstract: We present ab initio calculations (generalized valence bond plus configuration interaction, using relativistic effective core potentials) on the monopositive diatomic metal hydride ions of the third transition-metal series (HfH^+ through HgH^+ plus BaH^+ and LaH^+). We analyze the trends in bond energies, equilibrium geometries, bond character, and excitation energies in terms of (1) the atomic configuration of the metal, (2) the orbital sizes of the metal, and (3) the exchange and promotion energies on bonding hydrogen to the high-spin metal. The bond dissociation energies are found to be significantly larger than in either first- or second-row transition-metal hydride cations.

I. Introduction

Advances in experimental techniques[1] (in particular, guided ion-beam spectrometry) and in quantum chemical methods have led to increasingly accurate and consistent results for all first- and second-row transition-metal hydride cations. In reaching this level of accuracy, there has been a full partnership between experiment[2] and theory,[3] including mutual stimulation and verification. However, for third-row transition-metal (La–Hg) hydrides, there are little experimental or theoretical data available on bond energies and other properties.

In order to help stimulate experimental studies on these systems, we have extended the methods of previous investigations to the electronic structure of third-row transition-metal hydride cations. The results presented here should be a useful guide to forthcoming experiments. In addition, comparison of the bond energies and characteristics of *all* transition-metal hydrides provides global trends that may also apply to saturated complexes after appropriate corrections.[4]

In Sections II and III, the results for third-row metal hydrides (HfH^+ through HgH^+ plus BaH^+ and LaH^+) are presented and discussed with emphasis on the ground-state symmetries and configurations, bond distances, and bond energies. Comparison is made between the hydrides of all three transition-metal rows in Section IV. Section V compares our results with previous experimental and calculational studies. A brief summary is given in Section VI, and the calculational details are described in Section VII. As discussed in Section VII.D, relativistic effects play an important role for third-row metals. By using effective core potentials based on relativistic atomic calculations, we include the dominant relativistic effects. However, we average over spin–orbit coupling in discussing the valence states of MH^+. This allows us to more clearly distinguish the roles of the various atomic orbitals in the bonding.

II. Character of the Bond

We find that the major factors affecting the bonding of hydrogen to a transition-metal atom can be understood in terms of the atomic orbital configurations of the metal and the perturbation caused by spin-pairing to a hydrogen atom.

The metal properties to be considered are given below: (1) The first property is the relative energy and *orbital character of the low-lying metal atomic states*. Forming a covalent M^+–H bond requires a singly occupied metal orbital that overlaps the hydrogen 1s orbital. The stable orbital configuration of M^+ will determine whether the most readily available orbital for bonding is of s or d type. If an appropriate orbital is not available in the ground state, bond formation requires *promotion* to an excited configuration of M^+, thereby reducing the net bond energy. (2) The second property is *the size of the metal atomic orbitals*. The spatial extents of the valence orbitals (6s and 5d) are major factors determining the bond length. Their relative sizes must be close for optimum s–d hybridization to occur. The size of the outer core orbital (5p) places a repulsive wall to the approach of H, determining a minimum bond length.

The two main factors governing the bond energy are as follows: (3) The first factor is *the hybridization of the metal bonding orbital* [largely determined by factors 1 and 2 above]. This affects the bond energy because the intrinsic values for bonds of H to s and d orbitals are different. (Hybridization also influences the bond length because of the difference in size in 6s and 5d orbitals.) (4) The second factor is *the change in exchange energy of the nonbonding electrons*. Because the metal bond orbital is singly occupied and because M^+ generally has several such unpaired orbitals, its ground state is stabilized by favorable exchange interactions. However, spin-pairing the bond orbital of M^+ to the H will reduce the atomic exchange interactions with the nonbonding orbitals of M^+, reducing the bond energy.

In this paper, we present the results for third-row transition-metal hydrides in the light of the interplay of the above factors. Full details discussing these factors for first- and second-row systems have been provided in previous papers in this series,[3a-c] and we will summarize only the salient aspects here.

A. Orbital Configuration. The atoms of interest here have $(5d)^n$, $(6s)^1(5d)^{n-1}$, and $(6s)^2(5d)^{n-2}$ as low-lying valence configurations. Major factors determining which configuration is stable are (a) minimizing Coulomb repulsions (thus maximizing the number of singly occupied orbitals) and (b) maximizing the exchange interactions (thus maximizing the number of high-spin coupled open-shell electrons). The relative energies for the ground-state configurations[5,6] are shown in Table I and Figure 1. Despite the

† Permanent Address: Laboratoire de Chimie Théorique, Université de Paris Sud, 91405 Orsay, France.

‡ Current Address: Institute for Defense Analyses, Alexandria, VA 22311.

(1) Selected references include: (a) Elkind, J. L.; Armentrout, P. B. *J. Phys. Chem.* **1987**, *91*, 2037. (b) Tolbert, M. A.; Beauchamp, J. L. *J. Am. Chem. Soc.* **1984**, *106*, 8117. (c) Bartmess, J. E.; Kester, J. D. *Inorg. Chem.* **1984**, *23*, 1877. (d) Po, P. L.; Radus, T. P.; Porter, R. P. *J. Phys. Chem.* **1978**, *82*, 520.

(2) (a) Armentrout, P. B.; Georgiadis, R. *Polyhedron* **1988**, *7*, 1573. (b) Elkind, J. L.; Armentrout, P. B. *J. Phys. Chem.* **1987**, *91*, 2037. (c) Beauchamp, J. L. In *High Energy Processes in Organometallic Chemistry*; ACS Symposia Series No. 333; American Chemical Society: Washington, DC, 1987; Chapter 2. (d) Armentrout, P. B.; Beauchamp, J. L. *Acc. Chem. Res.* **1989**, *22*, 315.

(3) (a) Paper I: Schilling, J. B.; Goddard, W. A., III; Beauchamp, J. L. *J. Am. Chem. Soc.* **1986**, *108*, 582. (b) Paper II: Schilling, J. B.; Goddard, W. A., III; Beauchamp, J. L. *J. Phys. Chem.* **1987**, *91*, 5616. (c) Paper III: Schilling, J. B.; Goddard, W. A., III; Beauchamp, J. L. *J. Am. Chem. Soc.* **1987**, *109*, 5565. (d) Paper IV: Schilling, J. B.; Goddard, W. A., III; Beauchamp, J. L. *J. Phys. Chem.* **1987**, *91*, 4470. (e) Pettersson, L. G. M.; Bauschlicher, C. W., Jr.; Langhoff, S. R.; Partridge, H. *J. Chem. Phys.* **1987**, *87*, 481. (f) Alvarado-Swaisgood, A. E.; Harrison, J. F. *J. Phys. Chem.* **1988**, *92*, 2757. Also references in these papers.

(4) Carter, E. A.; Goddard, W. A., III *J. Phys. Chem.* **1988**, *92*, 5679.

(5) Moore, C. E. *Atomic Energy Levels*; National Bureau of Standards: Washington, D. C., 1971; Vol. III.

(6) van Kleef, Th. A. M.; Metsch, B. C. *Physica* **1978**, *95C*, 251. A theoretical analysis of the spectrum of Ir^+ and other third-row transition-metal cations can be found in: Wyart, J.-F. *Opt. Pura Apl. (Spain)* **1977**, *10*, 177.

0002-7863/90/1512-7179$02.50/0

Table I. Experimental and Theoretical State Splittings for Low-Lying States of Metal Cations[d]

	$6s^15d^{n-1}$		$5d^n$					$6s^25d^{n-2}$				
					relative energy,[a] eV					relative energy,[a] eV		
ion	state	config	state	config	HF	HF*SD	exper[b]	state	config	HF	HF*SD	exper[b]
Ba^+	^2S	$6s^1$	^2D	$5d^1$	0.95	0.95	0.65					
La^+	^3D	$6s^15d^1$	^3F	$5d^2$	−0.22	−0.22	−0.20	^1S	$6s^2$	1.18	0.60	0.57
Hf^+	^4F	$6s^15d^2$	^4F	$5d^3$	1.99	1.94	1.87	^2D	$6s^25d^1$	0.43	−0.31	−0.56
Ta^+	^5F	$6s^15d^3$	^5D	$5d^4$	1.68	1.62	1.47	^3F	$6s^25d^2$	1.38	0.79	0.43
W^+	^6D	$6s^15d^4$	^6S	$5d^5$	0.53	0.44	0.41	^4F	$6s^25d^3$	2.44	1.65	
Re^+	^7S	$6s^15d^5$	^5D	$5d^6$	3.57	2.64		^5D	$6s^25d^4$	4.39	2.94	1.83
Os^+	^6D	$6s^15d^6$	^4F	$5d^7$	2.15	1.56		^6S	$6s^25d^5$	0.56	0.49	
Ir^+	^5F	$6s^15d^7$	^3F	$5d^8$	1.07	0.55	0.28[c]	^5D	$6s^25d^6$	2.15	2.05	
Pt^+	^4F	$6s^15d^8$	^2D	$5d^9$	−0.09	−0.73	−0.76	^4F	$6s^25d^7$	3.02	2.93	2.79
Au^+	^3D	$6s^15d^9$	^1S	$5d^{10}$	−2.23	−2.48	−2.29	^3F	$6s^25d^8$	3.88	3.86	
Hg^+	^2S	$6s^15d^{10}$						^2D	$6s^25d^9$	6.12	5.78	5.15

[a] Relative energy with respect to the $6s^15d^{n-1}$ state. [b] Reference 5. The energies were calculated by using a weighted average over J levels for each state. [c] Splitting between the lowest J levels of the two states; see ref 6. [d] We show the lowest state with ($6s^15d^{n-1}$, $5d^n$, $6s^25d^{n-2}$) configurations (averaged over spin-orbit levels). The ground state is shown in boldface.

Table II. Valence Orbital Sizes (Å) for Third-Row Transition-Metal Ions[a]

		R(5d)						
		$5d^{n-1}4s^1$		$5d^n$			change on forming MH^+ bond	
ion	R(6s)	$(1e^-)^b$	$(2e^-)^b$	$(1e^-)^b$	$(2e^-)^b$	R(5p)	$R_e - R$(6s)	$R_e - R(5p_z)$
Ba^+	2.60			1.66		1.10	−0.40	1.10
La^+	2.37	1.60		1.65		1.03	−0.28	1.06
Hf^+	1.91	1.30		1.37		0.77	−0.12	1.02
Ta^+	1.80	1.19		1.26		0.74	−0.06	1.01
W^+	1.73	1.12		1.15		0.71	−0.03	0.99
Re^+	1.69	1.04		1.08	1.12	0.69	−0.03	0.97
Os^+	1.64	0.99	1.02	1.03	1.06	0.67	−0.03	0.94
Ir^+	1.61	0.95	0.96	0.98	1.00	0.65	−0.05	0.91
Pt^+	1.59	0.90	0.91	0.92	0.95	0.63	−0.07	0.89
Au^+	1.56	0.86	0.88		0.90	0.61	−0.02	0.93
Hg^+	1.52		0.83				+0.11	

[a] $R = (\langle\phi|r^2|\times\phi\rangle)^{1/2}$. [b] $1e^-$ and $2e^-$ indicate singly and doubly occupied orbitals.

importance of spin–orbit coupling, we discuss these states in terms of Russell–Saunders (LS) coupling, allowing a direct comparison of the three rows of transition metals.

For M^+, the s^2d^{n-2} configuration is usually of high energy (the s^2d^1 ground configuration of Hf^+ is an exception as discussed below), so that the ground state of MH^+ is generally constructed from either d^n or s^1d^{n-1}. Since d^n and s^1d^{n-1} are often close in energy, the ground molecular state sometimes involves a mixture of these configurations, allowing s and d character to blend in the bond orbitals. As for the first- and second-row metals, the leading trend is that the d^n configuration is preferentially stabilized when the d shell is either nearly half-filled or nearly completely filled [this occurs because of favorable exchange interactions (d–d exchange being larger than s–d)].

The lanthanide contraction, however, occurs as an additional factor for the third metal row. The compact 4f shell of orbitals is filled between lanthanum and hafnium, leading to a spectacular tightening of the s orbitals (the 6s size decreases from 2.37 to 1.91 Å from La^+ to Hf^+; see Table II) that arises from two effects: (a) differential shielding is more important for the s orbitals having non-zero amplitude at the nucleus, and (b) the importance of relativistic effects (which lead to a tightening of the s orbitals). This contraction of the s orbitals leads to more efficient screening of the nucleus from the d electrons, so that the d orbitals tighten less significantly (the 5d contracts from 1.60 to 1.30 Å from La^+ to Hf^+) and are less stabilized. The net effect is to stabilize the s^1d^{n-1} and s^2d^{n-2} states relative to the d^n. This has important consequences on atomic spectra: (i) Hf^+ is one of only two cases (the other is Y^+) of a transition-metal cation with a s^2d^{n-2} ground state, and (ii) the ground state of W^+ is s^1d^4 rather than d^5, contrary to its triad congeners Cr^+ and Mo^+. The "half-filled shell" effect is overwhelmed in W^+ by the differential stabilization of the s orbital. Compared to the other metal rows, the d^n state is relatively destabilized from Hf^+ to Hg^+. As a result of these factors, the third-row hydride bonds generally have much more s character than their second-row analogues.

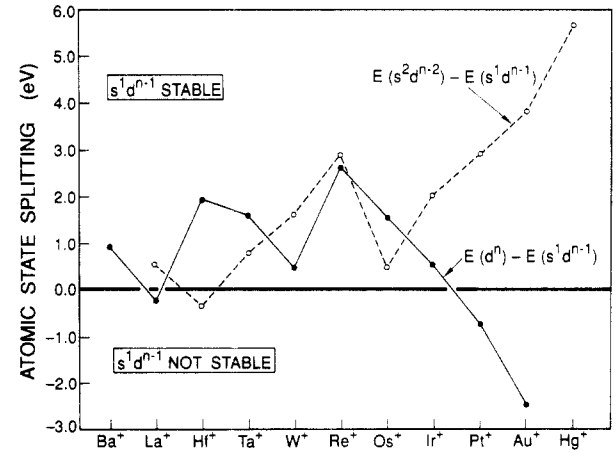

Figure 1. Energy difference between the lowest metal cation electronic states arising from the d^n and s^1d^{n-1} configurations (solid line) and from the d^n and s^2d^{n-2} configurations (dashed line). [$\Delta E = E_{d^n} - E_{s^1d^{n-1}}$ (solid line) and $\Delta E = E_{d^n} - D_{s^2d^{n-2}}$ (dashed line).] The experimental states have been averaged over J to obtain LS state energies.

An important concept in understanding the characteristic differences in the bond energies of first-, second-, and third-row TM's is contragradience.[9] Analysis of the bonding for GVB wave

(7) The p percentages are probably underestimated due to a somewhat less adequate p basis. If so, both s and d character would be slightly overestimated.
(8) Goddard, W. A., III; Harding, L. B. *Annu. Rev. Phys. Chem.* **1978**, *29*, 363.

(9) (a) Brusich, M. J.; Goddard, W. A., III, to be published. (b) Brusich, M. J. Ph.D. Thesis, California Institute of Technology, 1988 unpublished. (c) Steigerwald, M. L. Ph.D. Thesis, California Institute of Technology, 1983. (d) Wilson, C. W., Jr.; Goddard, W. A., III *Theor. Chim. Acta* **1972**, *26*, 195. (e) Goddard, W. A., III; Wilson, C. W. Jr. *Ibid.* **1972**, *26*, 211.

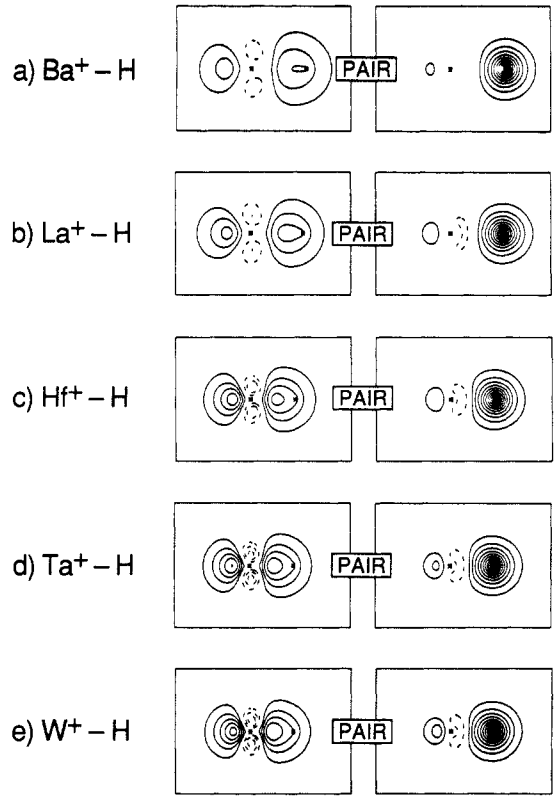

Figure 2. GVB bonding orbitals at R_e for (a) BaH^+, (b) LaH^+, (c) HfH^+, (d) TaH^+, and (e) WH^+. Solid lines indicate positive amplitudes while dotted lines indicate negative amplitudes. The spacing between contours is 0.05 au. The contours are plotted in the xz plane, with the M^+–H bond along the z axis. The plot limits are −3.0 to +4.0 Å for the z axis and −2.5 to +2.5 Å for the x axis.

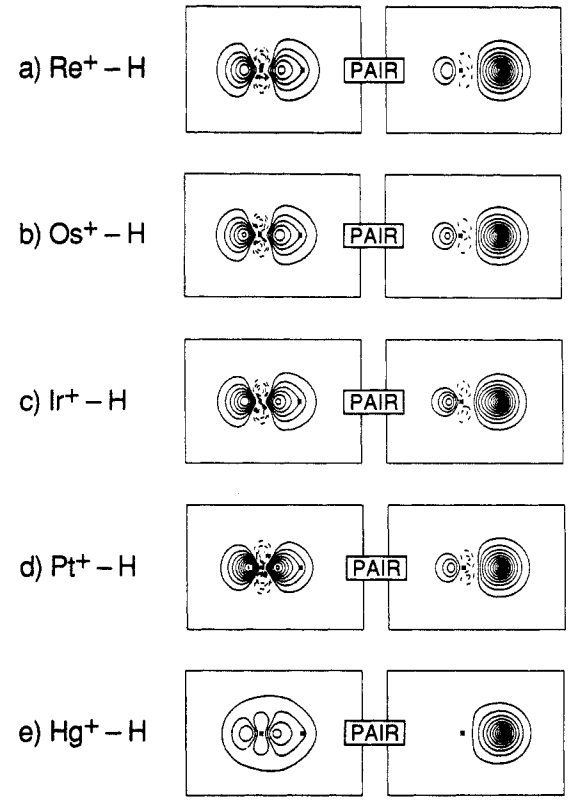

Figure 3. GVB bonding orbitals at R_e for (a) ReH^+, (b) OsH^+, (c) IrH^+, (d) PtH^+, and (e) HgH^+. The plotting parameters are the same as for Figure 2.

functions shows that the strength of a covalent bond involving, say, ϕ_M and ϕH is related to the decrease in kinetic energy that results when the orbitals are spin-paired [leading to $(\phi_M\phi_H + \phi_M\phi_H)(\alpha\beta - \beta\alpha)$]. This decrease in kinetic energy (called contragradience[9]) arises from regions where the slope (gradient) of ϕ_M is opposite that of ϕ_H and is largest if the magnitudes of the slopes are equal. This region is located between the hydrogen and the outer maximum of ϕ_M (the bond region) and is largest if ϕ_M has low amplitude in other regions. If ϕ_M is an s orbital, it is distributed over all angles around M and has a slope smaller than that of ϕ_H. For example, the bond energy in alkali hydrides

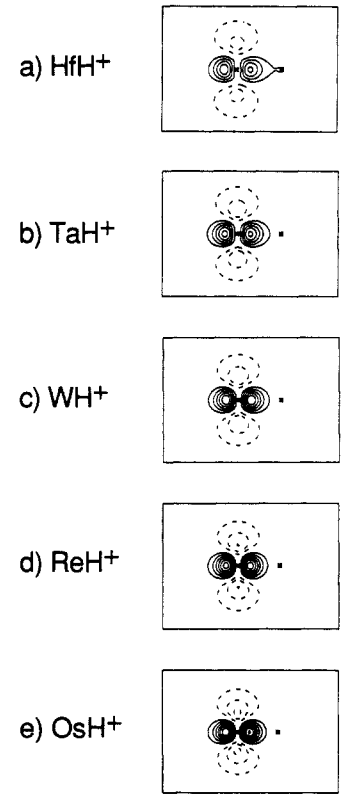

Figure 4. GVB nonbonding σ orbitals at R_e for (a) HfH^+, (b) TaH^+, (c) WH^+, (d) ReH^+, and (e) OsH^+. The plotting parameters are the same as for Figure 2.

(10) Pyykkö, P. *J. Chem. Soc., Faraday Trans. 2* **1979**, *75*, 1256.
(11) Pyykkö, P.; Snijders, J. G.; Baerends, E. J. *Chem. Phys. Lett.* **1981**, *83*, 432.
(12) Fuentealba, P.; Reyes, O. *Mol. Phys.* **1987**, *62*, 1291.
(13) Wang, S. W.; Pitzer, K. S. *J. Chem. Phys.* **1983**, *79*, 3851.
(14) Elkind, J. L.; Sunderlin, L. S.; Armentrout, P. B. *J. Phys. Chem.* **1989**, *93*, 3151.
(15) Huber, K. P.; Herzberg, G. *Molecular Spectra and Molecular Structure. IV. Constants of Diatomic Molecules*; Van Nostrand Reinhold: New York, 1979.
(16) (a) Mrozowski, A. S. *Phys. Rev.* **1940**, *58*, 332. (b) Herzberg, G. *Spectra of Diatomic Molecules*; Van Nostrand Reinhold: New York, 1950. (c) Gaydon, A. G. *Dissociation Energies*; Chapman and Hall: London, 1968.
(17) Georgiadis, R.; Armentrout, P. B. *J. Phys. Chem.* **1988**, *92*, 7060.
(18) Ziegler, T.; Snijders, J. G.; Baerends, E. J. *J. Chem. Phys.* **1981**, *74*, 1271.
(19) Ramos, A. F.; Pyper, N. C.; Malli, G. L. *Phys. Rev.* **1988**, *A38*, 2729.
(20) Hay, P. J.; Wadt, W. R. *J. Chem. Phys.* **1985**, *82*, 299.
(21) Hay, P. J.; Wadt, W. R. *J. Chem. Phys.* **1985**, *82*, 270.
(22) (a) Huzinaga, S. *J. Chem. Phys.* **1965**, *42*, 1293. (b) Dunning, T. H., Jr. *J. Chem. Phys.* **1970**, *43*, 2823.
(23) (a) Bair, R. A.; Goddard, W. A., III, to be published. (b) Bair, R. A. Ph.D. Thesis, California Institute of Technology, 1981. (c) Carter, E. A.; Goddard, W. A., III *J. Chem. Phys.* **1988**, *88*, 3132.
(24) Bobrowicz, F. B., Goddard, W. A., III In *Modern Theoretical Chemistry: Methods of Electronic Structure Theory*; Schaefer, H. F., III, Ed.; Plenum Press: New York, 1977; Vol. 3, Chapter 4.
(25) (a) Ladner, R. C.; Goddard, W. A., III *J. Chem. Phys.* **1969**, *51*, 1073. (b) Moss, B. J.; Bobrowicz, F. W.; Goddard, W. A., III *Ibid.* **1975**, *63*, 4632.
(26) Reference deleted in press.
(27) Goddard, W. A., III *Phys. Rev.* **1967**, *157*, 73, 81.
(28) Ohanessian, G.; Goddard, W. A., III, to be published.
(29) Balasubramanian, K. *J. Phys. Chem.* **1989**, *93*, 6585.

Table III. Character of Wave Functions for MH^+ from GVB-PP(1/2) Calculations

molecule[a]	state	character of metal bonding orbital[b] % s	% p	% d	overlap[c]	charge transfer to H
BaH^+ (d^0)	$^1\Sigma^+$	34.5	1.6	63.9	0.76	0.41
LaH^+ (d^1)	$^2\Delta$	22.6	1.6	75.8	0.74	0.30
HfH^+ (d^2)	$^3\Delta$	34.8	0.9	64.3	0.76	0.26
TaH^+ (d^3)	$^4\Sigma^-$	39.1	0.9	60.0	0.75	0.19
WH^+ (d^4)	$^5\Pi$	40.6	0.7	58.6	0.74	0.15
ReH^+ (d^5)	$^6\Sigma^+$	42.4	0.7	56.9	0.73	0.10
OsH^+ (d^6)	$^5\Pi$	43.1	0.6	56.3	0.73	0.05
IrH^+ (d^7)	$^4\Sigma^-$	36.7	0.4	62.9	0.76	0.04
PtH^+ (d^8)	$^1\Sigma^+$	10.6	0.3	89.1	0.67	−0.04
AuH^+ (d^9)	$^2\Sigma^+$	29.8	0.2	70.0	0.78	−0.02
HgH^+ (d^{10})	$^1\Sigma^+$	91.4	2.0	6.5	0.69	−0.11

[a] Nonbonded d orbital occupation given in parenheses. [b] Defined as the Mulliken population in s, p, and d metal basis functions in the GVB orbital centered on the metal atom. [c] Overlap between the two nonorthogonal GVB orbitals describing the σ bond.

decreases going down the periodic table (from 56.0 kcal/mol for LiH, 43.4 kcal/mol for NaH, to 41.7 kcal/mol for CsH). If ϕ_M is a d_{z^2} orbital, it is concentrated along the z axis, with a large slope toward the H, both favorable for contragradience. For the 3d orbital the slope is much larger than for ϕ_H, but it decreases from 3d to 4d to 5d. Thus the contragradience and strength of the intrinsic d bond (ignoring promotion and exchange effects) increases going down the periodic table. Hybridizing the 4s and 3d orbitals can increase the contragradience, leading to an optimum[9c] for about 40% s and 60% d.

The GVB bonding orbitals for third-row hydrides are shown in Figures 2 and 3 and analyzed in Table III. Selected nonbonding σ orbitals are also shown in Figure 4. These results indicate that d bonding remains a strong component in third-row hydrides (close to the values in the second row) and that the s bonding is more significant at the expense of less participation of p orbitals to the bond.[7] Also, from Table III we find that the charge transfer from M^+ to H is fairly limited (average of 0.15 electron for the whole series), leading to essentially covalent bonds (as found for the other two series). On the basis of the charge transfer in MH^+ bonds, we see the following trends: (a) early atomic cations (groups 2–6) become more electropositive when going down the periodic table, (b) group 7 cations transfer about the same charge to H, (c) groups 8–10 have the second-row metal the most electronegative, and (d) for groups 11 and 12 the trend is completely reversed, with the metal becoming more *electronegative* when going down the table.

The late transition-metal cations (groups 7–10) show a quite dramatic alternation in character. For the first row (as indicated in Figure 10), the bonds involve mainly metal s character (~13% d). This is because the d orbitals are particularly small (no d core electrons), making the s shell much more readily available for bonding. The 5s and 4d orbitals of second-row metals have a more similar size and the bonding is largely d in character (~81% d) because d^n is stabilized. However, in the third row the bonds have more nearly equal s and d character (66% d) because s is stabilized (vide supra).

B. Orbital Size and Bond Length. The sizes of atomic s and d orbitals influence the bond lengths in hydrides. As discussed above, for first-row metals the d orbitals are much tighter than the s, but this difference is less important for the second and third rows (where valence s and d orbitals both have underlying core orbitals of the same symmetry). Due to the lanthanide contraction (see Table II and ref 3c), the 6s orbitals of third-row metals are slightly tighter than the 5s in the second row, while the opposite is true for 5d versus 4d.

On the other hand, a trend common to all three rows is the tightening of orbitals when going from early to late metals. Thus the sizes of the 6s orbitals diminish from 1.91 Å for Hf^+ to 1.56 Å for Au^+, while the 5d's drop from 1.30 Å in Hf^+ to 0.86 Å in Au^+. The stronger tightening of 5d relative to 6s between Hf^+ and Au^+ is due to the lower principal quantum number (5 versus 6). A second-order effect is that the mutual shielding among d orbitals is much less effective than their shielding of the 6s orbital. This differential shielding effect also tends to make the d contraction greater than the s. Considering the full row starting with Ba^+, the lanthanide contraction counteracts these effects, making the total s and d contractions very similar.

These orbital contraction effects cause a general decrease of the metal–hydrogen bond distance along the row. The best correlation is between the size of the 6s atomic orbital and the MH^+ bond length (see Table II), where the bond length is consistently about 0.05 Å smaller than the 6s orbital from HfH^+ to AuH^+. A close correspondence of the hydride length with the size of the valence s orbital was also observed for the first and second rows (see Figure 9).

Another way to analyze the MH^+ bond length is to note that the hydrogen is prevented from approaching the metal atom too closely by the repulsive wall (Pauli orthogonalization) due to the outer core orbitals, among which 5p is the largest. In Table II we see that the size of this orbital drops by 0.49 Å from Ba^+ to Hg^+, while the bond distance in MH^+ drops by 0.58 Å. The equilibrium bond length for MH^+ is about 1.0 Å larger than the size of the $5p_z$ orbital (Table II) for the whole row. It is interesting that these trends are so similar for all three rows despite the characteristic changes in bond character.[3a-c]

Table IV. Spectroscopic Properties of Ground-State MH^+

molecule	state	bond length R_e, Å	force const[a] k_e, mdyn/Å	vibr freq ω_e, cm^{-1}	bond energies,[b] kcal/mol D_0	D_e
BaH^+	$^1\Sigma^+$	2.202	1.168	1408	50.9	52.9
LaH^+	$^2\Delta$	2.093	1.350	1513	60.4	62.6
HfH^+	$^3\Delta$	1.786	2.313	1979	54.9	57.7[b]
TaH^+	$^4\Sigma^-$	1.741	2.376	2006	54.0	56.9
WH^+	$^5\Pi$	1.701	2.517	2065	49.9	52.9
ReH^+	$^6\Sigma^+$	1.659	2.518	2065	44.5	47.5
OsH^+	$^5\Pi$	1.605	2.975	2244	56.2	59.4
IrH^+	$^4\Sigma^-$	1.560	3.323	2372	65.8	69.2
PtH^+	$^1\Sigma^+$	1.519	3.400	2399	62.9	66.3
AuH^+	$^2\Sigma^+$	1.539	3.050	2273	33.4	36.6
HgH^+	$^1\Sigma^+$	1.627	2.108	1888	48.6	51.3

[a] Divide by 4.3598 to obtain hartree/Å^2 or multiply by 143.93 to obtain (kcal mol^{-1})/Å^2. [b] Including f functions (optimized exponent: 0.39) leads to D_e = 60.7 kcal/mol.

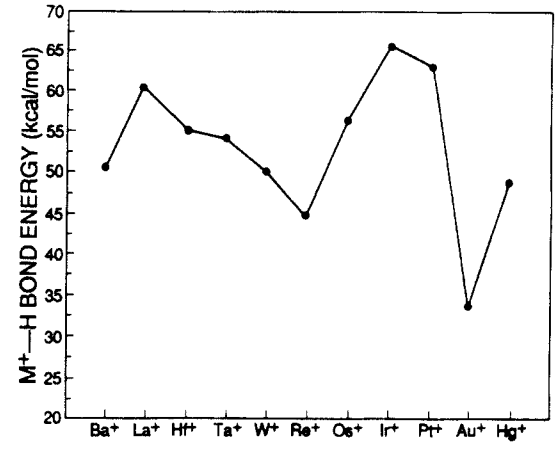

Figure 5. Calculated bond energies (D_0) for third-row transition-metal hydride cations.

III. Dissociation

A. Bond Energies. Having clarified the factors that shape the electronic character and bond length of MH^+, we turn now to the bond strength. The spectroscopic characteristics of the ground state of each hydride are reported in Table IV. The bond dissociation energies are also shown in Figure 5 and comparison with the other rows in Figure 11. The rather complex pattern of Figure

Table V. 6s–5d and 5d–5d Exchange Energies for Re^+ (from the Atomic Hartree–Fock Wave Function)

	$^7S(6s^15d^5)$		$^5S(5d^6)^a$	
orbitals	no. of terms	K, kcal/mol	no. of terms	K, kcal/mol
s–d	5	11.9	0	
av d–d	10	14.1	6	14.9
d_σ–d_π	2	10.8	0	
d_σ–d_δ	2	17.4	0	
d_π–d_π	1	15.2	1	16.1
d_π–d_δ	4	15.2	4	16.0
d_δ–d_δ	1	8.7	1	9.1

[a] d_{z^2} doubly occupied; all other d orbitals singly occupied.

5 emphasizes the fact that several effects are at work in determining these bond energies.

There are two major determinants (points 3 and 4 in Section II.A):

(i) The first is the hybridization of the metal bonding orbital (mixing of 6s and $5d_\sigma$ character). Table III shows that all M^+–H bonds are dominated by d contributions (89% for PtH^+ and 56–75% for the others) except HgH^+ (which has 7%). It is interesting to note that the ground state of PtH^+ (with only a single σ electron on Pt^+) chooses to be 89% d character (11% s), in reasonable agreement with PdH^+ (93% d, 5% s). This is related to the stability of the ^2D (d^9) state of group 10 metal cations. The size of these bonds (relative to the valence s orbitals) seems relatively constant for the elements of groups 8, 9, and 10 [$R_e - R(5s) = +0.01$ for the first row, $R_e - R(5s) = -0.13$ for the second row, $R_e - R(6s) = -0.05$ for the third row (see Table II)].

(ii) The second is the loss of exchange energy among metal electrons upon spin pairing with the hydrogen orbital.[8] Since the ground state of the metal ion tends to have the highest possible spin (Hund's rule), the loss of exchange energy between the bonding and nonbonding electrons increases from 0 in BaH^+ to $2.5K_{dd'}$ in ReH^+ (increment of $0.5K_{dd'}$), and then decreases again to finally reach 0 in HgH^+ (increment of $-0.5K_{dd'}$). Since $K_{dd'}$ is about 15 kcal/mol in third-row metals (values for Re^+ are given in Table V), the exchange energies are important in determining the bond energies.

While point i above concerns the electrons directly involved in the bond, point ii arises from the interaction with the nonbonding orbitals.

The general pattern of bond energies across the third row is roughly the same as for first- and second-row hydrides (see Table IV and Figure 5). The effect of exchange loss is very clear, making the ReH^+ bond the weakest of the whole series (except for the special case of AuH^+) and leading to intermediate weakening in WH^+ and OsH^+. There are, however, some significant differences in the bond energy patterns of the three series of hydrides. The case of group 6 metal hydrides is illustrative of such differences. The bond in CrH^+ was found to be particularly weak because of the promotion energy (d^5 to s^1d^4) required for Cr^+ to make an s-like bond to H. In MoH^+, the bond is mainly d-like and therefore the $^6S(d^5)$ ground state is adequate for bonding. However, the exchange loss is $2K_{dd'}$ in MoH^+ instead of $2K_{sd}$ as in CrH^+, leading to a weak bond for Mo^+–H. In contrast, W^+ has a $^6D(s^1d^4)$ ground state so that the WH^+ bond can have either large s or large d components without the need for promotion. In addition, $K_{dd'}$ and K_{sd} are comparable so that the exchange loss does not bias the hybridization. Thus the character of the W^+–H bond reflects the optimal hybridization, and the net bond is significantly stronger than for CrH^+ or MoH^+. As a consequence, the weakest bond in the third series (except for AuH^+) is not for the group 6 metal, as in the first two rows, but for group 7 (ReH^+) in which the exchange loss is a maximum.

The case of AuH^+ is peculiar because the ground state of Au^+ is d^{10} which has no singly occupied orbital available for bonding. Thus the bond to H *requires* promotion to the excited $^3D(s^1d^9)$ state.

Making corrections for promotion energy and exchange loss (see Figure 6) leads to an *intrinsic* bond energy, D^{int}, that varies smoothly within each row[30] (see Figure 6). This intrinsic bond energy is significantly larger for third-row hydrides than for the two other series. This increase for third-row hydrides occurs because the similarity in size of the 6s and 5d orbitals allows an optimal combination of 6s and 5d to achieve large contragradience between the metal and H orbitals[9] (slopes in opposite direction in the bond region), which leads to a large decrease in the kinetic energy upon spin pairing, and hence a strong bond.[9] [The 6s orbitals in the third row are tighter than the 5s in the second row.] Thus ref 9c showed that 60% d is optimum if all exchange and promotion effects are ignored, and we find ~60% for most MH^+ cases (see Table III). The overall effect is a significant increase in the bond strength for the third row.

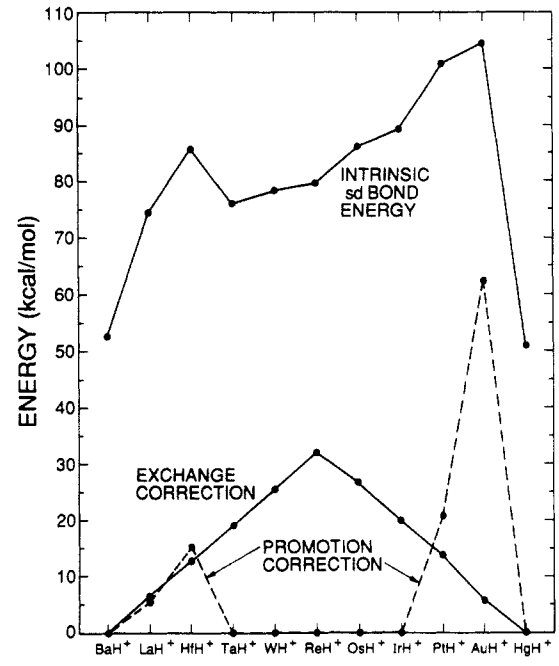

Figure 6. Exchange and promotion energy corrections to the bond energy of the ground state. The intrinsic bond energy is after correcting for exchange and promotion effects.

The promotion correction assumes that the bonding state is pure s^1d^{n-1}, which leads to an upper bound. Thus, for AuH^+ assuming that the bonding state is pure s^1d^9 leads to a promotion energy of 62 kcal (Figure 6). In fact (vide infra) the optimal wave function obtains more bonding by mixing with d^{10}, leading to a smaller promotion energy.

B. Spin Coupling. The GVB wave function[24,25,27] for ReH^+ has the form

$$C_1 \begin{vmatrix} s + d\sigma & Hs \\ s - d\sigma \\ d\pi_x \\ d\pi_y \\ d\delta_{xy} \\ d\delta_{x^2-y^2} \end{vmatrix} + C_2 \begin{vmatrix} s + d\sigma & Hs \\ s - d\sigma \\ d\pi_x \\ d\pi_y \\ d\delta_{xy} \\ d\delta_{x^2-y^2} \end{vmatrix} \quad (1)$$

(1a) (1b)

where the ratio of C_1 and C_2 determines the spin coupling, which is calculated simultaneously with optimizing the orbitals in (1). [The orbitals are labeled by their dominant character; however, they are allowed to mix with any orbital on either center.] Component 1a denotes a GVB wave function that has singlet pairing of the ($s + d_\sigma$) and H s orbitals to form the bond, while the other five valence orbitals on Re^+ are coupled high-spin ($S = {}^5/_2$). The component 1b denotes a GVB wave function in which

(30) For Au^+ the intrinsic bond energy is quoted as 63 kcal/mol, a value that is too large. This results because our analysis assumes that the state of Au^+ in AuH^+ is pure s^1d^9, whereas the actual wave function involves a mixture of d^{10} and s^1d^9.

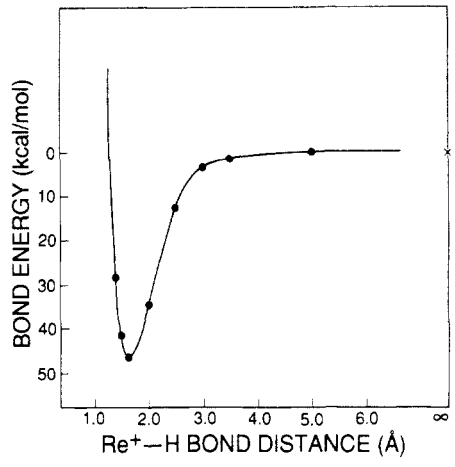

Figure 7. Potential energy curve for the ground state of ReH^+ with CCCI/D. The point at infinite R is from separate calculations on Re^+ and H.

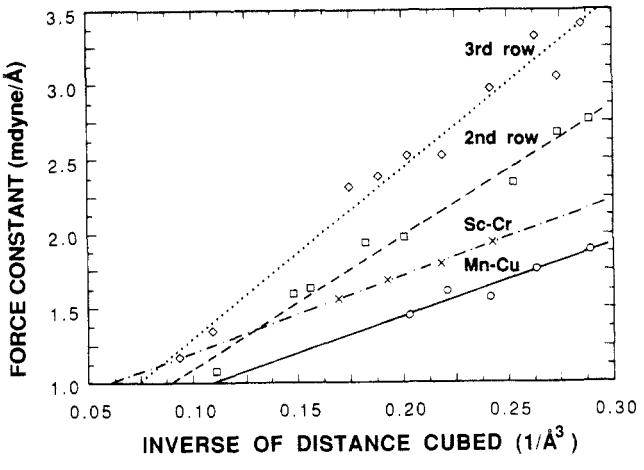

Figure 8. Validity of the Badger rule relationship between force constant (k_e) and $1/R_e^3$ for third-row transition-metal hydrides. The points are from calculations; the line is Badger's rule: $k_e = A + B/R_e^3$.

all six Re^+ orbitals are coupled high-spin ($S = 3$) and then coupled to the H s orbital to obtain a net spin of $S = {}^5/_2$. Component 1b also leads to bonding, but the total strength of the bond is about ${}^1/_6$ of that in (1a) [the six arises[27] because the (s + d_σ) orbital is coupled high-spin to five other orbitals].

Near R_e the high overlap of the Re^+ (s + d_σ) and H s orbitals favors configuration 1a and the wave function has $C_1 \approx 1$ and $C_2 \approx 0$, which was assumed in the above discussion of exchange energy effects. However, as R increases and the overlap of Re^+ and H decreases, the potential strength of the bond pair becomes less than the exchange energy loss associated with (1a). Thus for longer R, C_1 decreases and C_2 increases so that eventually $C_1 = 0$ and $C_2 = 1$ for $R = \infty$. As the spin coupling changes, the orbitals change smoothly into the optimum orbitals of Re^+ ($S = 3$) and H and the total energy changes smoothly to the energy of the ground-state atoms, as indicated in Figure 7.

Since the wave function at R_e corresponds to (1a), the potential curve near R_e has the shape as if the energy would dissociate to an excited state of Re^+ (a mixture of $S = 2$ and 3). As a result, the vibrational frequency ω_e and the spectroscopic properties of ReH^+ do *not* correlate with the bond energy D_e (which involves dissociation to the ground state of Re^+). This is clear in Table IV where, for example, HfH^+, TaH^+, WH^+, and ReH^+ all have $\omega_e \approx 2000$ cm^{-1} *but* D_e changes from 58 to 48 kcal/mol. Similarly, OsH^+ and AuH^+ have $\omega_e \approx 2260$ cm^{-1} *but* $D_e = 59$ and 37 kcal/mol, respectively.

C. Badger's Rule. On the other hand, the R_e and $k_e = M\omega_e^2$ *do* correlate (inversely) with each other since both are properties of the potential energy near R_e. Indeed, k_e and R_e satisfy Badger's rule: $k_e \approx A + B/R_e^3$, where A and B are constants for M^+ = La$^+$, Hf$^+$–Au$^+$. In Figure 8 we show the Badger rule correlations for all three rows. Each row is well fit with a constant value of B (which increases as one goes down a column); however, for the first row there is a drop in A between CrH^+ and MnH^+ (where the character of the bond changes dramatically from[3a] ~40% d to ~13% d). The values of A and B are tabulated in Table XI.

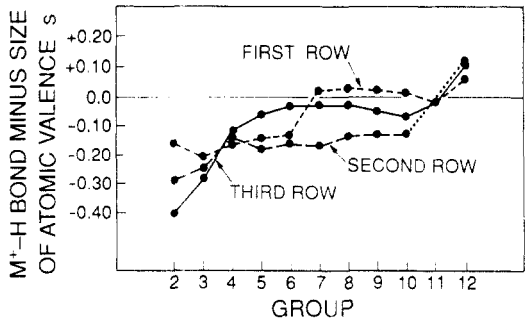

Figure 9. Sizes of metal valence s and d atomic orbitals. The size is defined as $(\langle\phi|r^2|\phi\rangle)^{1/2}$ from Hartree–Fock calculations.

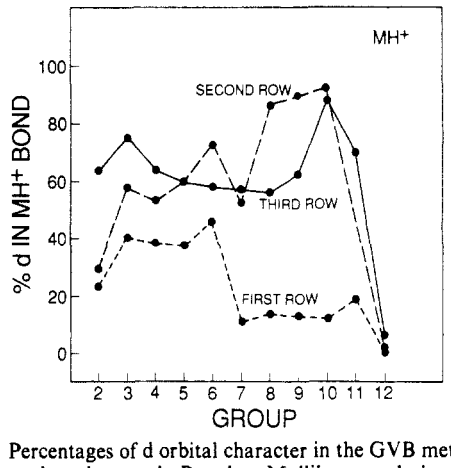

Figure 10. Percentages of d orbital character in the GVB metal bonding orbital centered on the metal. Based on Mulliken populations where the total on the atom is normalized.

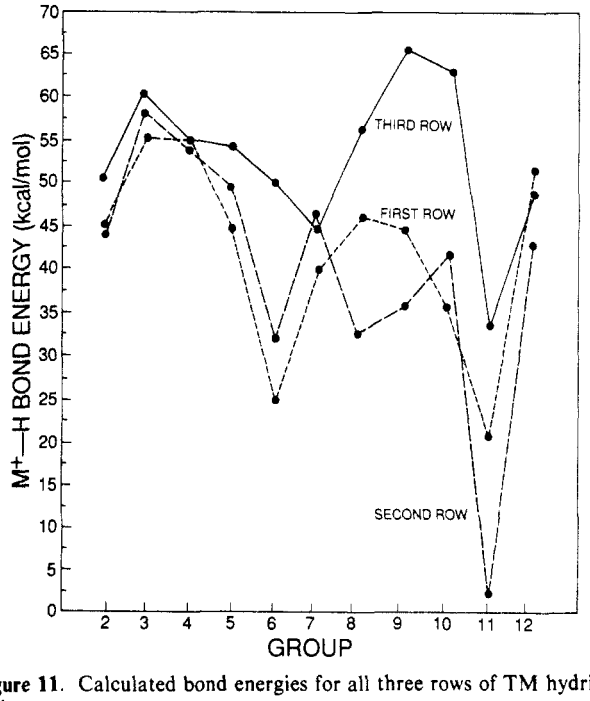

Figure 11. Calculated bond energies for all three rows of TM hydride cations.

IV. Low-Lying MH^+ Electronic States

Another consequence of the lanthanide contraction concerns the occupation of the nonbonding orbitals. For the first-row

Table VI. Comparison of the Low-Lying State of the TM Hydrides for All Three Rows of the Periodic Table

group	state	first row	second row	third row
3		ScH^+	YH^+	LaH^+
	$^2\Delta$	0.0	8.3	0.0
	$^2\Pi$	5.1	15.2	8.9
	$^2\Sigma^+$	8.0	0.0	5.9
4		TiH^+	ZrH^+	HfH^+
	$^3\Phi$	0.0	0.0	23.2
	$^3\Sigma^-$	2.9	2.3	25.4
	$^3\Pi$	3.9	3.8	11.4
	$^3\Delta$	11.6	1.5	0.0
5		VH^+	NbH^+	TaH^+
	$^4\Delta$	0.0	0.0	17.5
	$^4\Pi$	4.5	1.9	5.9
	$^4\Sigma^-$	12.1	8.7	0.0
	$^4\Phi$	13.8	10.0	0.9
6		CrH^+	MoH^+	WH^+
	$^5\Sigma^+$	0.0	0.0	4.7
	$^5\Delta$		25.1	1.5
	$^5\Pi$		37.2	0.0
7		MnH^+	TcH^+	ReH^+
	$^6\Sigma^+$	0.0	0.0	0.0
	$^4\Delta$		24.0	
	$^4\Pi$		26.4	
8		FeH^+	RuH^+	OsH^+
	$^5\Delta$	0.0	6.7	7.6
	$^5\Pi$	2.1	9.0	0.0
	$^5\Sigma^+$	10.0	15.7	10.3
	$^3\Sigma^-$		0.0	40.3
	$^3\Phi$		0.2	38.9
	$^3\Pi$		9.0	35.0
9		CoH^+	RhH^+	IrH^+
	$^4\Phi$	0.0		3.8
	$^4\Sigma^-$	1.3		0.0
	$^4\Pi$	6.4		11.1
	$^4\Delta$	14.4		26.6
	$^2\Delta$	17.6	0.0	20.8
	$^2\Pi$		19.5	
10		NiH^+	PdH^+	PtH^+
	$^3\Delta$	0.0		1.0
	$^3\Pi$	8.7		19.3
	$^1\Sigma^+$	9.1	0.0	0.0
	$^3\Sigma^-$	18.4		
	$^3\Phi$	18.9		45.4
11		CuH^+	AgH^+	AuH^+
	$^2\Sigma^+$	0.0	0.0	0.0
	$^2\Delta$		80.3	
	$^2\Pi$		81.5	

hydrides, we found the following picture to predict the low-lying state orbital configuration: The hydrogen is spin-paired with a singly occupied metal σ orbital to form a two-electron covalent σ bond, leading a variable number of nonbonding electrons on the metal (from zero for group 2 to ten for group 12). The nonbonding electrons prefer δ or π orbitals to minimize electrostatic repulsion with the σ pair. For atoms with only one σ orbital occupied on M^+, the mixing of 6s and $5d_\sigma$ is optimized for the bond to H. This holds for group 2 to group 6, where all nonbonding electrons can be accommodated in singly occupied π or δ orbitals. Beginning with the d^5 nonbonding configuration (group 7), there must be at least one nonbonding electron in the σ orbital. As additional electrons are added, there must be doubly occupied nonbonding orbitals, but the π and δ orbitals are again filled before d_σ. Table VI compares the energies of the low-lying state for all the TM rows. Thus for ScH^+–CuH^+ the nonbonding occupations are

$$d_\sigma^0 d_{\pi\delta}^1, d_\sigma^0 d_{\pi\delta}^2, d_\sigma^0 d_{\pi\delta}^3, d_\sigma^0 d_{\pi\delta}^4, d_\sigma^1 d_{\pi\delta}^4, d_\sigma^1 d_{\pi\delta}^5, d_\sigma^1 d_{\pi\delta}^6, d_\sigma^1 d_{\pi\delta}^7, d_\sigma^1 d_{\pi\delta}^8 \quad (2)$$

where we have grouped d_π and d_δ together.

For the second row the same picture emerges, except that because of the extra stabilization of the 4d versus 5s orbitals, the ground states of Ru^+, Rh^+, and Pd^+ strongly prefer d^n configurations. The result is that YH^+–PdH^+ have the nonbonding occupations

$$d_\sigma^0 d_{\pi\sigma}^1, d_\sigma^0 d_{\pi\delta}^2, d_\sigma^0 d_{\pi\delta}^3, d_\sigma^0 d_{\pi\delta}^4, d_\sigma^1 d_{\pi\delta}^4, (d_\sigma^0 d_{\pi\delta}^6), (d_\sigma^0 d_{\pi\delta}^7), (d_\sigma^0 d_{\pi\delta}^8) \quad (3)$$

where the cases that differ from the first row are in parentheses. AgH^+ is not listed since the strong preference of Ag^+ d^{10} leads to essentially no bond.

In contrast the description for the third row is strongly perturbed by the stabilization of s orbitals following the lanthanide contraction. The result is that most ground states of third-row TM cations are s^1d^{n-1}, with s^2d^{n-2} states also relatively stable. Thus, after forming the MH^+ bond, the bias in favor of σ orbital occupation in the hydrides leads HfH^+, TaH^+, and WH^+ to occupy the d_σ nonbonding orbital, even though d_π and d_δ are available. The result is that for LaH^+ and HfH^+–AuH^+ the nonbonding occupations are

$$d_\sigma^0 d_{\pi\delta}^1, (d_\sigma^1 d_{\pi\delta}^1), (d_\sigma^1 d_{\pi\delta}^2), (d_\sigma^1 d_{\pi\delta}^3), d_\sigma^1 d_{\pi\delta}^4, d_\sigma^1 d_{\pi\delta}^5, d_\sigma^1 d_{\pi\delta}^6, (d_\sigma^0 d_{\pi\delta}^8), d_\sigma^1 d_{\pi\delta}^8 \quad (4)$$

where again the cases differing from the first row are in parentheses.

With the third row there are also differences in the occupations of d and d_δ orbitals, which we will now examine in more detail. To help follow the discussion, the nonbonding orbital occupations are given in Table VII, , along with a summary of results for all states calculated in this work.

The group 3 hydride cations have one nonbonding electron. On the basis of the repulsion of this electron with the bond pair, one

Table VII. Relative Energies and Spectroscopic Properties of Some Low-Lying Metal Hydride Electronic States

molecule	state	nonbond config $d\sigma$	$d\pi$	$d\delta$	bond length R_e, Å	vib freq ω_e, cm^{-1}	rel energy, kcal/mol
BaH^+	$^1\Sigma^+$	0	0	0	2.202	1408	0.0
LaH^+	$^2\Delta$	0	0	1	2.093	1513	0.0
	$^2\Sigma^+$	1	0	0	2.060	1562	5.9
	$^2\Pi$	0	1	0	2.083	1493	8.9
HfH^+	$^3\Delta$	1	0	1	1.786	1979	0.0
	$^3\Pi$	0	1	1	1.779	1898	11.4
		1	1	0			
	$^3\Phi$	0	1	1	1.829	2220	23.2
	$^2\Sigma^-$	0	2	0	1.831	1775	25.4
		0	0	2			
TaH^+	$^4\Sigma^-$	1	2	0	1.741	2006	0.0
		1	0	2			
	$^4\Phi$	1	1	1	1.727	2030	0.9
	$^4\Pi$	0	1	2	1.740	1964	5.9
		1	1	1			
	$^4\Delta$	0	2	1	1.763	2376	17.5
WH^+	$^5\Pi$	1	1	2	1.701	2065	0.0
	$^5\Delta$	1	2	1	1.678	2227	1.5
	$^5\Sigma^+$	0	2	2	1.707	2032	4.7
ReH^+	$^6\Sigma^+$	1	2	2	1.659	2065	0.0
OsH^+	$^5\Pi$	1	3	2	1.605	2244	0.0
	$^5\Delta$	1	2	3	1.638	2182	7.6
	$^5\Sigma^+$	2	2	2	1.640	2111	10.3
	$^3\Pi$	0	3	3	1.602	2301	35.0
	$^3\Phi$	0	3	3	1.602	2261	38.9
	$^3\Sigma^-$	0	4	2	1.597	2211	40.3
		0	2	4			
IrH^+	$^4\Sigma^-$	1	4	2	1.560	2372	0.0
		1	2	4			
	$^4\Phi$	1	3	3	1.583	2265	3.8
	$^4\Pi$	1	3	3	1.593	2269	11.1
		2	3	2			
	$^2\Delta$	0	4	3	1.545	2426	20.8
	$^4\Delta$	2	2	3	1.656	1996	26.6
PtH^+	$^1\Sigma^+$	0	4	4	1.519	2399	0.0
	$^3\Delta$	1	4	3	1.531	2445	1.0
	$^3\Pi$	1	3	4	1.587	2268	19.3
		2	3	3			
	$^3\Phi$	2	3	3	1.624	2042	45.4
AuH^+	$^2\Sigma^+$	1	4	4	1.539	2273	0.0
HgH^+	$^1\Sigma^+$	2	4	4	1.627	1812	0.0

would expect the ordering $^2\Delta$ (lowest), $^2\Pi$, $^2\Sigma^+$, as found for ScH^+. For LaH^+ $^2\Delta$ is the ground state but $^2\Sigma^+$ is below $^2\Pi$, whereas YH^+ has a $^2\Sigma^+$ ground state. The reason is that the atomic state splittings differ significantly between Sc^+, Y^+, and La^+, leading to corresponding changes in the state ordering for MH^+. In particular, the $^1S(s^2)$ state, which is of high energy in Sc^+, is the ground state of Y^+ and is of moderately high energy in La^+ [0.77 eV above the $^3F(d^2)$ ground state]. Bonding the H atom to one of the lobes of the ^1S state leads to the $^2\Sigma^+$ ground state of YH^+ (with three σ electrons). This explains why $^2\Sigma^+$ is the ground state of YH^+ but the first excited state of LaH^+ (below the $^2\Pi$). On the other hand, the relative ordering of $^2\Delta$ and $^2\Pi$ remains unchanged in all three cases.

The effect of the lanthanide contraction begins with HfH^+ and brings with it some significant changes in the state energies. The ground state of Hf^+ is $^2D(s^2d^1)$, while Ti^+ and Zr^+ are $^4F(s^1d^2)$. Consequently, the ground state of HfH^+ is $^3\Delta$ with σ and δ nonbonding electrons. The first excited state is $^3\Pi$ arising from a mixing of s^2d^1 (using s and d_π nonbonding orbitals) and s^1d^2 (using d_π and d_δ nonbonding orbitals). The remaining two states, $^3\Phi$ and $^3\Sigma^-$, arise from s^1d^2. The $^3\Delta$ state of MH^+ is steadily stabilized relative to all others when going down the group 4 column of the periodic table, being, respectively, the third excited state in TiH^+, the first one in ZrH^+, and the ground state of HfH^+. For the three other states, the energy ordering is $^3\Phi$, $^3\Sigma^-$, $^3\Pi$ in TiH^+ and ZrH^+ but changes to $^3\Pi$, $^3\Phi$, $^3\Sigma^-$ in HfH^+, as discussed above.

The low-lying states of VH^+ and NbH^+ are similar, reflecting the similarity in the spectra of the atomic cations [$^5D(d^4)$ ground state, with the $^5F(s^1d^3)$ state low-lying (0.34 and 0.33 eV in V^+ and Nb^+, respectively)]. The basic rule was found to be the following: spin-pair the H to a σ metal orbital while not allowing the nonbonding electrons to be σ. Thus, $^4\Delta$, the only state meeting this requirement, was found to be the ground state. The massive stabilization of s-occupied states that occurs in Ta^+ makes $^5F(s^1d^3)$ the ground state [with $^3F(s^2d^2)$ 0.43 eV higher] and $^5D(d^4)$ quite high (1.47 eV above ^5F). As a result, TaH^+ has a $^4\Sigma^-$ ground state ($\sigma\pi^2$ nonbonding orbitals mixed with $\sigma\delta^2$ nonbonding orbitals), with $^4\Phi(\sigma\pi\delta)$ nearly degenerate.

The differences in spectra between WH^+, MoH^+, and CrH^+ are particularly striking due to the spectacular reversal of the state ordering in the metal atomic cations. The $^6S(d^5)$ state is significantly lower in energy than $^6D(s^1d^4)$ for both Cr^+ and Mo^+ due to the half-filling of the d shell (the energy difference being 1.52 and 1.59 eV, respectively), leading to a $^5\Sigma(\pi^2\delta^2)$ ground state for MH^+. In W^+, however, the ^6D state is 0.44 eV *lower* than ^6S, leading to stabilization of the $^5\Delta(\sigma\pi^2\delta)$ and $^5\Pi(\sigma\pi\delta^2)$ states of WH^+ (which have a σ nonbonding electron). While $^5\Sigma^+(\pi^2\delta^2)$ is the most stable by far in both CrH^+ and MoH^+, all three states are close in WH^+.

The $^7S(s^1d^5)$ state of the group 7 metal cations is strongly stabilized as the ground state because of optimal exchange coupling of all six electrons. The $^5D(s^2d^4)$ state is 1.81 and 0.51 eV higher in Mn^+ and Tc^+ and 2.6 ± 0.2 eV higher for Re^+. [The experimental splitting is not known for Re^+; the uncertainty of 0.2 eV in the computed value of 2.64 eV is based on the accuracy of these calculations for other metal cations for the third series.] As a result, all three have $^6\Sigma^+(\sigma^1\pi^2\delta^2)$ ground states.

The ground state of Os^+ is $^6D(s^1d^6)$ with $^6S(s^2d^5)$ lying 0.49 eV higher, while the $^4F(d^7)$ state is 1.56 eV above ^6D. As a result, the three quintet states ($^5\Pi$, $^5\Delta$, and $^5\Sigma^+$) of OsH^+ arising from s^1d^6 are strongly favored over the three triplet states ($^3\Pi$, $^3\Phi$, and $^3\Sigma^-$) arising from d^7. The exact reverse is true in RuH^+, where the ground state of Ru^+ is $^4F(d^7)$, with ^6D 1.09 eV higher. For Fe^+ the ground state is s^1d^6 (^6D) but d^7 (^4F) is only 0.25 eV higher! Thus the ground state of FeH^+ is quintet, as with OsH^+. [The triplet states of FeH^+ were not calculated but are expected to be higher than the quintets since FeH^+ favors s^1d^6.]

Among the low-lying OsH^+ quintets, $^5\Sigma^+$ is the highest because of its doubly occupied σ nonbonding orbital. It is interesting that $^5\Pi$ [with nonbonding configuration $(d_\sigma)^1(d\pi)^3(d\delta)^2$] is the ground state of OsH^+ with $^5\Delta$ [nonbonded configuration $(d_\sigma)^1(d_\pi)^2(d_\delta)^3$] lying 7.6 kcal/mol higher, whereas for RuH^+ and FeH^+, the $^5\Delta$ state is 2.3 and 2.1 kcal/mol *below* $^5\Pi$. For s^1d^6, the atomic configurations $(d_\sigma)^1(d_\pi)^3(d_\delta)^2$ and $(d_\sigma)^1(d_\pi)^2(d_\delta)^3$ have the same energy, but bonding a σ orbital to the H leads to a coulombic interaction with H that favors double occupation of d_δ over d_π, leading to a $^5\Delta$ ground state. The special characteristic of Os^+ is that s^2d^5 is very low-lying (0.49 eV for the s^1d^6/s^2d^5 excitation energy compared with 3.19 eV in Ru^+). The orbital configuration from s^2d^5 that can mix with the s^1d^6 configuration is $s^2(d_\pi)^3(d_\delta)^2$ for $^5\Pi$, while $^5\Delta$ requires $(d_\pi)^2(d_\delta)^3$. The first configuration has a lower energy [this is easy to see since $(d_\sigma)^1(d_\pi)^3(d_\delta)^2$ and $(d_\sigma)^1(d_\pi)^2(d_\delta)^3$ have the same energy but $J_{\sigma,\pi} > J_{\sigma,\delta}$], stabilizing the $^5\Pi$ state.

Co^+ has a d^8 ground state [with $s^1d^7(^5F)$ lying 0.43 eV higher], but the preference for 4s character in the bond leads to quartet of ground and low-lying states that arise from Co^+ s^1d^7. For Ir^+ the ground state is $^5F(s^1d^7)$ [with $^3F(d^8)$ 0.55 eV higher], leading to states similar to CoH^+ [$^4\Sigma^-(\sigma^1\pi^4\delta^2)$ ground state with $^4\Phi(\sigma^1\pi^3\delta^3)$ low lying]. However, Rh^+ (which has d^8 favored by 2.13 eV) is quite different, leading to doublet states: $^2\Delta(d_\pi^4d_\delta^3)$ is the ground state and $^2\Pi(d_\pi^3d_\delta^4)$ is the first excited state, with no low-lying quartets.

For Pt^+, Pd^+, and Ni^+, the d^9 state is most stable. This leads to a ^1S state for PdH^+ and PtH^+, both involving a d_σ bond to H. However, for NiH^+ (as with the other first-row hydrides), the d_σ orbital is too small for good overlap. As a result, Ni^+ is promoted to the $^4F(s^1d^8)$ state, leading to a bond to the 4s orbital and a $^3\Delta$ ground state ($\sigma^1\pi^4\delta^3$). For Pt^+, the low-lying s^1d^8 state leads to the $^3\Delta$ state only 1 kcal/mol above $^1\Sigma^+$, while in Pd^+ the large splitting between d^9 and s^1d^8 makes the $^3\Delta$ state of PdH^+ of high energy.

For the noble metals the ground state of M^+ is d^{10}, leading to a $^2\Sigma^+$ nonbonding state for MH^+. Forming a covalent bond requires promotion to s^1d^9, and in all three cases the ground state involves significant mixing of d^{10} and s^1d^9, leading to the $^2\Sigma^+$ ground state. The $^2\Delta$ and $^2\Pi$ states arising from s^1d^9 [but with nonbonding configurations ($\sigma^2\pi^4\delta^3$) and ($\sigma^2\pi^3\delta^4$), respectively] are expected to lie much higher (the have two σ nonbonding electrons). Indeed, calculations on AgH^+ place them over 80 kcal/mol above the ground state.[3c]

The bonding is much simpler in group 12 hydrides since the metal cations have a ^2S (s^1d^{10}) ground state, leading to MH^+ bond orbitals that are almost exclusively of s character on the metal. With no promotion energy to pay but no d contribution to the bonds, group 12 hydrides have moderately strong bond energies.

V. Comparison with Previous Work

A. Experiment. The only third-row transition-metal hydride cations for which there are experimental data are LaH^+ and HgH^+. Recent guided ion beam experiments by Armentrout et al.[14] yielded a bond energy of 57.2 ± 2.0 kcal/mol for LaH^+, in good agreement with our calculated value of 60.4 kcal/mol.

For HgH^+, the experimental bond length[15] of 1.594 Å is in satisfactory agreement with our calculated value of 1.627 Å. However, there may be a problem with the bond energy, which we calculate as D_e = 51.3 kcal/mol. The experimental bond energy is based on experiments carried out in the 1930's.[16a] The 1979 review by Huber and Herzberg[15] quotes D_e = 69.3 kcal/mol, the 1968 Gaydon review[16c] quotes D_e = 67 ± 14 kcal/mol, whereas the 1950 review by Herzberg[16b] quotes D_e = 53 kcal/mol. The most recent experimental paper (1940) quotes D_e = 49.6 kcal/mol, which is in agreement with our calculations. Thus a reexamination of the experimental bond energy for HgH^+ is in order.

The trends in the MH^+ bonds for the group 12 metals support the theoretical results for HgH^+. In these systems the bond between H and a group 12 metal cation (Zn^+, Cd^+, or Hg^+) is largely s in character (since M^+ is s^1d^{10}). Thus the bond lengths and bond energies should correlate with the size of the valence s orbital. The atomic orbital sizes are 1.49 Å (4s of Zn^+), 1.60 Å (5s of Cd^+), and 1.52 Å (6s of Hg^+), with Hg^+ intermediate between Zn^+ and Cd^+ (because of the lanthanide contraction and relativistic effects). We therefore expect both bond length and

bond strength to follow the trend $CdH^+ < HgH^+ < ZnH^+$. This is obtained for the bond lengths (calculated as 1.545, 1.627, and 1.709 Å, respectively, and measured experimentally as 1.514, 1.594, and 1.67 Å). The calculated bond energies also follow this trend (42.0 kcal/mol for CdH^+, 48.5 kcal/mol for HgH^+, and 52.4 kcal/mol for ZnH^+). This is also the case for the experimental values of CdH^+ (49.3 kcal/mol) and ZnH^+ (57.7 kcal/mol, recently remeasured to be 54.4 kcal/mol[17]). But for HgH^+, use of the value D_e = 69.3 kcal/mol would disobey the trend, while use of D_e = 53.0 kcal/mol *would* satisfy it.

B. Theory. The first calculation on third-row transition-metal hydride cations seems to be that of Pyykkö[10] (BaH^+ and HgH^+). Using a Dirac–Fock one-center expansion (DFOCE), he calculated bond energies of 37.0 and 84.7 kcal/mol (without and with d functions, respectively) for BaH^+, with equilibrium geometries of 2.849 and 2.272 Å, respectively. These should be compared with our values of 52.9 kcal/mol and 2.202 Å. Using local density functions with (first-order) relativistic effects on BaH^+, Pyykkö et al.[11] found bond lengths of 2.43 and 2.24 Å [without and with d functions] but no bond energies were reported. The most recent calculations on BaH^+ are those of Fuentealba and Reyes,[12] who carried out a local spin density functional calculation of the valence electrons with a relativistic effective potential (including core polarization). Their results of R_e = 2.243 and 2.137 Å and D_e = 47.7 and 52.8 kcal/mol (fitting the core potential to all electron calculations or to experiment, respectively) are in reasonable agreement with those of the present work (2.202 Å and 52.9 kcal/mol).

Wang and Pitzer[13] performed a relativistic Hartree–Fock calculation on PtH^+ at the equilibrium geometry of PtH (1.61 Å). They obtained a bond energy of 25.9 kcal/mol for the $^3\Delta$ ground state. At our optimized geometry for PtH^+ (1.519 Å), we find a $^1\Sigma^+$ ground state with a bond energy of 66.3 kcal/mol (22.3 kcal/mol at the GVB-PP level), but the adiabatic transition energy to the $^3\Delta$ state is only 1.0 kcal/mol.

For HgH^+, Pyykkö,[10] using DFOCE, calculated a bond length of 1.808 Å and a bond dissociation energy of 27.6 kcal/mol (our values are 1.627 Å and 51.1 kcal/mol). Ziegler et al.,[18] using local density functional theory and a perturbative treatment of relativistic effects, obtained a bond distance of 1.64 Å, a bond energy of 62 kcal/mol, and a vibrational frequency of 2156 cm^{-1} (we calculate 1812 cm^{-1}). More recently, Ramos et al.,[19] performing ab initio Dirac–Fock calculations, obtained a bond energy of 15.2 kcal/mol at the experimental bond distance.

VI. Summary

We find that GVB calculations followed by correlation-consistent CI (CCCI/D) lead to a *consistently accurate* description of the spectroscopic properties of the third-row transition-metal hydrides and that the GVB orbitals lead to a qualitative interpretation that explains most variations observed in the states for hydrides of the first- second-, and third-row transition metals. These ideas should also be useful in predicting the states of other transition-metal compounds (oxides, nitrides, methylidenes, methyls, etc.).

The higher M^+–H dissociation energies found for the third-row hydrides make it plausible that oxidative addition of H_2 is an exothermic process. (Until now, only group 3 metal cations have been observed to insert into the H–H bond.) Recent calculations[28] on IrH_2^+ and $Ir(CH_3)_2^+$ provide support for this idea.

VII. Calculational Details

A. Basis Sets and Effective Potentials. In all cases but Hg, the 46 electrons associated with the n = 1, 2, 3, and 4 metal-core orbitals have been replaced with the ab initio effective core potentials of Hay and Wadt[20] (HW), which include relativistic effects for the core electrons. Thus, the 5s, 5p, 5d, 6s, and 6p shells are considered explicitly. The basis set is contracted valence double-ζ (5s5p3d/3s3p2d). However, we found that the contraction of HW leads to a systematic bias in favor of the d^n configurations over s^1d^{n+1} and s^2d^{n-2} for M^+. This is because the basis set was determined for neutral atoms, while the orbitals of the positive ions are more contracted (differential shielding effects are more important for s than d orbitals, see Section II). Consequently, we recontracted the valence s functions as follows. Keeping the HW (5/1) contraction for the core, we dropped the inner gaussian from the valence space and contracted the valence s functions (4/31) from a restricted Hartree–Fock calculation on the cation. We then dropped the outer two gaussians from the core functions, which we considered too diffuse (having rather small coefficients). This contraction scheme was found to yield atomic state splittings in substantially better agreement with calculations using the full uncontracted basis set and with experiment. The resulting s bases are listed in the Table VIII.

Table VIII. The *s* Basis Sets Used for Third-Row Transition Metals[a]

	Ba^+		Re^+		Hg^+	
0.8699	−2.291032	2.1850	−1.637201	0.5275	1	
0.6676	2.554787	1.4510	2.012088	0.2334	1	
0.1982	0.586753	0.4585	0.457258	0.0686	1	
0.6676	−0.033	1.4510	−0.078			
0.1982	−0.552	0.4585	−0.552			
0.0823	0.979	0.2314	0.973			
0.0231	1	0.0566	1			
	La^+		Os^+			
0.9167	−3.026804	0.2220	−1.664305			
0.7427	3.300122	1.4960	2.080155			
0.2237	0.551852	0.4774	0.425889			
0.7427	−0.073	1.4960	−0.094			
0.2237	−0.397	0.4774	−0.530			
0.0792	1.061	0.2437	0.991			
0.0239	1	0.0583	1.0			
	Hf^+		Ir^+			
1.9500	−1.233434	2.3500	−1.689732			
1.1830	1.578915	1.5820	2.109321			
0.3897	0.496298	0.5018	0.419088			
1.1830	−0.052	1.5820	−0.101			
0.3897	−0.484	0.5018	−0.482			
0.1656	0.897	0.2500	0.962			
0.0424	1	0.0598	1			
	Ta^+		Pt^+			
2.0440	−1.319247	2.5470	−1.484838			
1.2670	1.669087	1.6140	1.925735			
0.4157	0.488078	0.5167	0.395138			
1.2670	−0.077	1.6140	−0.103			
0.4157	−0.395	0.5167	−0.522			
0.1671	0.876	0.2651	1.027			
0.0482	1	0.0580	1			
	W^+		Au^+			
2.1370	−1.404508	2.8090	−1.203037			
1.3470	1.767249	1.5950	1.675385			
0.4366	0.473814	0.5327	0.352918			
1.3470	−0.086	1.5950	−0.111			
0.4366	−0.422	0.5327	−0.532			
0.1883	0.917	0.2826	1.029			
0.0518	1	0.0598	1			

[a] Spaces are used to separate primitives for different contracted basis functions.

Since the HW basis for Ba^+ does not include d functions, we optimized a set of two uncontracted 5d functions for BaH^+ (using full valence CI). The starting geometry was R = 2.4612 Å, the optimum bond length for GVB-PP(1/2) without d's. The exponents optimized at this geometry are 0.3586 and 0.1280. The bond length was then reoptimized, including these two d functions in the basis. At the new optimal bond length of 2.225 Å, the d exponents were reoptimized, leading to final values of 0.3595 and 0.1297.

For Hg^+, the HW effective potential[21] has the full Xe core (54 electrons) replaced by the effective potential (leaving 11 electrons to be considered explicitly). Using the contracted double-ζ basis as suggested by HW, we found a strong bias in favor of the $^2S(s^1d^{10})$ state versus the $^2D(s^2d^9)$ state. Consequently, we left the three s and p gaussians uncontracted for all calculations on HgH^+. The atomic ^2S–^2D splittings are 6.29, 5.69, 5.78, and 5.82 eV, respectively, for the four basis sets: (a) HW double-ζ, (b) s uncontracted bases, (c) s and p uncontracted, and (d) HW fully uncontracted. The experimental value is 5.15 eV. Contracting the p functions to double-ζ resulted in a decrease in the bond energy for HgH^+ from 51.3 to 48.1 kcal/mol.

Table I shows a comparison between the available experimental state splittings for third-row transition metals and those obtained with our basis sets. As discussed below, the configurations used in the CI were restricted Hartree–Fock times all single and double excitations to the virtual space (HF*SD).

For hydrogen, we used the unscaled Huzinaga/Dunning[22] triple-ζ basis (6s/3s) supplemented with one set of p polarization functions of exponent 0.6.

F polarization functions were not systematically added to the metal ion bases. To estimate the effects on the bond dissociation energies of including f functions, one set of f functions was optimized for HfH^+ (α = 0.39) using the Correlation-Consistent Configuration Interaction (CCCI)/S level of calculation (see below) at the optimum geometry of the ground state. The polarization functions were found to increase the bond energy (calculated at the CCCI/D level) by 3.0 kcal/mol. An analogous increase would be expected for the other third-row metal hydrides.

B. Wave Functions and Electron Correlation. For the third-row metal hydrides, we used generalized valence bond (GVB) wave functions[24] and dissociation-consistent configuration interaction as for the first- and second-row compounds.[3a-c] That is, emphasis was put on treating both the molecule and the separated fragments at consistent levels of theory, and correlation energy is recovered mainly for those electrons that change between the molecular and atomic limits. There are some differences, however, since additional correlation terms were taken into account in the present work.

To optimize the bond lengths and compute the bond dissociation energies, we used the following approach. We started with the CCCI/S wave function, defined as follows: (a) We begin with the two spatial configurations of a GVB-PP(1/2) wave function, where the bonding electrons form the GVB pair. (b) We then carry out a restricted CI in the bond pair orbitals, RCI(1/2), where all three occupations of the two GVB orbitals are allowed for the two bonding electrons and where all spin couplings are allowed. The RCI(1/2) wave function dissociates smoothly to describe M^+ and H at the Hartree–Fock level. (c) Starting with the GVB-RCI configurations, we allow all single and double excitations (SD) from the bond pair to all possible virtual and occupied orbitals [denoted as $RCI(1/2)^*SD_{bond}$]. Allowing SD excitations from the bond pair fully correlates this electron pair and leads to a dissociated limit where the M^+ ion is described as Hartree–Fock times all single excitations of the "bonding" electron. (d) In addition, the CCCI/S wave function allows relaxation of the nonbonding orbitals in the following way. We allow all single excitations out of all nonbonding orbitals from the three configurations of the RCI(1/2) wave function [denoted as $RCI(1/2)^*S_{val}$].

The total wave function comprising terms (a), (b), (c), and (d) is denoted as $RCI(1/2)^*[SD_{bond} + S_{val}]$ or more simply as CCCI/S. It dissociates to the HF*S limit for M^+ (and for H) as the atoms are pulled apart. (This wave function was denoted DCCI-GEOM in previous papers in this series.[3a-d])

We have now improved upon the CCCI/S wave function for two reasons: (1) We found that HF*S does rather poorly on the atomic state splittings. For example, it causes bias for systems in which the character of the wave function at R_e corresponds to an excited state of M^+. For instance, the ^2D ground state of Hf^+ involves a dominant s^2d^1 configuration with the $^4F(s^1d^2)$ 0.56 eV higher, but HF*S would introduce a strong bias in favor of s^1d^2 (since it has no doubly occupied orbitals) and place ^4F 0.43 eV *below* ^2D. (2) The intrapair correlation of the nonbonding electrons, which is not included in CCCI/S, has an influence on the bond properties for late metal hydrides (since several nonbonding orbitals are doubly occupied). For example, in AuH^+, where the SCF configuration is s^1d^9 on the metal but a large amount of d^{10} builds in the CI wave function (see Section II), it is important to let the nonbonding electron pairs readjust to obtain a balanced mixture of s^1d^9 and d^{10} characters. For some first- and second-row hydrides, Pettersson et al.[3e] found that including such terms leads to bond distances 0.05–0.07 Å shorter than those obtained with CCCI/S wave functions.

Our improved wave function CCCI/D differs from CCCI/S in that we replace (c) and (d) by the following: (c′) same as (c) but allow all single and double excitations out of the bond pair times all single excitations from the nonbonding electrons [denoted $RCI(1/2)^*SD_{bond}{}^*S_{val}$], and (d′) same as (d) but allow all double excitations from the RCI wave function [denoted $RCI(1/2)^*D_{val}$]. This CCCI/D wave function [also denoted $RCI(1/2)^*(SD_{bond}{}^*S_{val} + D_{val})$] dissociates smoothly to M^+ at the HF*SD level plus a hydrogen atom. Since the HF*SD description of M^+ leads to good excitation energies, the CCCI/D should also lead to good excitation energies (see Table I). The reference configurations used in CCCI/D calculations are all those compatible with the above description, e.g., all four $\pi^1\delta^1$ for the $^3\Phi^+$ state of HfH^+, even though some are not of the proper symmetry. The symmetry constraints were imposed only *after* the generation of the full configuration list. This ensures a consistent level of correlation for states of all symmetries. The total energies for M^+ and MH^+ at the GVB-PP and CCCI/D levels of calculation are given in Table IX.

From Table I, we see that HF*SD on the metal cations does provide satisfactory atomic state splittings. This level should also provide better ionization potentials for the metal and therefore better describe the metal-to-hydrogen charge transfer in the hydrides. The DCCI level used in previous papers in this series corresponds to $RCI(1/2)^*SD_{bond}{}^*S_{val}$ and dissociates into M^+ involving HF*S plus some of the double excitations (only those involving the "bonding" electron and one of the nonbonding ones, thereby accounting for correlation between the bond pair and the nonbonding electrons, but not between nonbonding electrons).

C. Averaged Hamiltonian Calculations. When CI calculations are performed with a limited configuration list as detailed above, the final wave functions depend upon how the orbitals are optimized (step a). They can be optimized for each state separately (denoted GVB in Table X), or a common set of orbitals can be used for all states. Some states

Table IX. Total Energies of Ground-State MH^+, M^+, and H

species	state	total energies[a] GVB-PP	CCCI/D
BaH^+	$^1\Sigma^+$	−25.30325	−25.31557
Ba^+	^2S	−24.73130	−24.73130
LaH^+	$^2\Delta$	−31.17773	−31.19079
La^+	^3D	−30.59064	−30.59113
HfH^+	$^3\Delta$	−48.65047	−48.66945
Hf^+	^2D	−48.04865	−48.07748
TaH^+	$^4\Sigma^-$	−57.45714	−57.48625
Ta^+	^5F	−56.89095	−56.89557
WH^+	$^5\Pi$	−67.39051	−67.41803
W^+	^6D	−66.82789	−66.83373
ReH^+	$^6\Sigma^+$	−78.67093	−78.70563
Re^+	^7S	−78.12024	−78.12998
OsH^+	$^5\Pi$	−90.53920	−90.58665
Os^+	^6D	−89.97161	−89.99198
IrH^+	$^4\Sigma^-$	−104.07366	−104.18311
Ir^+	^5F	−103.54957	−103.57290
PtH^+	$^1\Sigma^+$	−118.52281	−118.58692
Pt^+	^2D	−117.93972	−117.98134
AuH^+	$^2\Sigma^+$	−134.78136	−134.84031
Au^+	^1S	−134.24594	−134.28210
HgH^+	$^1\Sigma^+$	−41.67069	−41.82215
Hg^+	^2S	−41.10940	−41.24042
H	^2S	−0.49994	−0.49994

[a] For MH^+ the total energies are for the calculational levels shown. For the M^+ and H the energies are for the calculational level to which the corresponding description of MH^+ dissociates. Thus, GVB-PP on MH^+ leads to HF on M^+ and CCCI/D on MH^+ leads to HF*SD on M^+ (see section III.B).

Table X. Relative Energies (eV) of the Low-Lying States of HfH^+ (R = 1.830 Å) with Various Starting Orbitals and Levels of CI

orbitals	CI	$^3\Delta$ $\sigma^1\delta^1$	$^3\Pi$ $\pi^1\delta^1$	$^3\Phi$ $\pi^1\delta^1$	$^3\Sigma^-$ π^2
GVB(1/2)[a]	FULL	0.00[d]	0.50	0.99	1.09
GVB(1/2)[a]	CCCI/S	0.00	0.51	0.98	1.06
GVB(1/2)[a]	CCCI/D	0.00	0.50	0.99	1.09
$\sigma^1\pi^{0.5}\delta^{0.5}$[b]	CCCI/S	0.00	0.50	0.98	1.07
$\sigma^1\pi^{0.5}\delta^{0.5}$[b]	CCCI/D	0.00	0.50	1.02	1.10
$\sigma^{0.4}\pi^{0.8}\delta^{0.8}$[c]	CCCI/S	0.00	0.49	0.96	1.05
$\sigma^{0.4}\pi^{0.8}\delta^{0.8}$[c]	CCCI/D	0.00	0.49	0.99	1.07

[a] For each state the CI uses the GVB(1/2) orbitals for the same state. [b] All states use the orbitals from the GVB Hamiltonian with nonbonding orbital occupancies $\sigma^1\delta_{x^2-y^2}^{0.25}\delta_{xy}^{0.25}\pi_x^{0.25}\pi_y^{0.25}$. [c] All states use the orbitals from the GVB Hamiltonian with nonbonding orbital occupancies $\sigma^{0.4}\delta_{x^2-y^2}^{0.4}\delta_{xy}^{0.4}\pi_x^{0.4}\pi_y^{0.4}$. [d] GVB(1/2) energy: −48.65024 hartrees. Full CI energy: −48.66903 hartrees.

Table XI. Constants from the Fits to Badger's Rule $k_e = A + B/R_e^3$

range	A, mdyn/Å	B, mdyn Å^2
ScH^+ – CrH^+	5.077	0.699
MnH^+ – CuH^+	4.841	0.477
YH^+ – PdH^+[a]	8.842	0.211
LaH^+, HfH^+ – AuH^+	11.378	0.163

[a] TcH^+ excluded.

require several configurations even for their basic description, and the simplest way to allow for the necessary flexibility is to use an averaged Fock hamiltonian. In this section, we provide more details about such calculations for the representative case of HfH^+, comparing the energy spectrum obtained by using different SCF and CI methods at the internuclear distance of 1.830 Å.

The expected low-lying states of HfH^+ are $^3\Delta(\sigma^1\delta^1)$, $^3\Pi(\pi^1\delta^1,\sigma^1\pi^1)$, $^3\Phi(\pi^1\delta^1)$, and $^3\Sigma^-(\pi^1\pi^1,\delta^1\delta^1)$, where the dominant configuration(s) of nonbonding electrons are given in parentheses but with the σ bond pair omitted for clarity. Orbitals based, say, on the GVB wave function for the $^3\Delta$ state would bias against all other states since they all involve a π orbital that would not be optimized self-consistently. In addition, the $^3\Pi$ and $^3\Sigma^-$ states require several types of reference configurations in the CI. Several averaged-field calculations were performed, and the resulting spectra are compared in Table IX at the CCCI/S and CCCI/D levels of CI. (As indicated, full CI (FCI) leads to essentially the same results.) Hamiltonian 1 consists of placing one electron in a σ orbital and 0.25 electron in each of the four remaining δ and π orbitals, while hamiltonian 2 involves 0.4 electron in each of the five orbitals. From Table X we see that the state splittings are not sensitive to the type of orbital since the variation (0.02 eV) is within the range of uncertainty due to using a truncated AO basis. It is encouraging that the calculational level used throughout this work (GVB orbitals adapted to each individual state plus CCCI/D) reproduces the full CI results to 0.01 eV. Lone-pair electron correlation effects in late transition metals might lead to less perfect matching, but the agreement is expected to remain satisfactory.

For some late metals, CCCI/S (which ignores the pair correlation of nonbonding electrons) leads to results significantly different from those obtained with CCCI/D. Thus, for IrH^+, CCCI/S leads to R_e = 1.572 Å and D_e = 64.9 kcal/mol, while CCCI/D leads to R_e = 1.560 Å and D_e = 69.2 kcal/mol.

D. Relativistic Effects and Spin-Orbit Coupling. The quantitative importance of relativistic effects grows very rapidly going down a column of the periodic table, and they are quite significant for the third transition row and beyond. The effective potentials[20,21] used in this study include the dominant relativistic terms (mass-velocity and Darwin) for the core electrons. Previous tests[20,21] and the present calculations of atomic splittings (Table I) and orbital sizes (Table II) indicate that these potentials are successful in taking into account the bulk of core relativistic effects. Thus Table II shows that both s and d orbitals undergo a spectacular tightening from La^+ to Hf^+, with the effect for the s orbital being larger than for d orbitals, as expected. On the other hand, for molecules formed from sixth-row atoms, valence spin-orbit effects are significant for states that are both orbitally degenerate *and* spin degenerate.[29] For such systems, our calculations represent the average over the spin-orbit sublevels. One can estimate these corrections by using the experimental spin-orbit splitting of the atom (M^+), which could be used to extract a spin-orbit coupling parameter $[E_{JLS}(M^+) = \lambda[J(J+1) - L(L+1) - S(S+1)]]$, which would be used as a perturbation, $\delta H = \lambda\hat{L}\cdot\hat{S}$ added to the normal electronic Hamiltonian to estimate the spin-orbit coupling of the molecular state (MH^+). Unfortunately, for the third row atoms the experimental atomic spectra are generally quite incomplete, and we have not attempted such corrections here.

Spin-orbit coupling can affect the ordering of the low-lying excited states. Generally states with high orbital angular molecular (Ω) and large spin will be favored. For example, the $^4\Phi$ state of TaH^+ is calculated only 0.9 kcal/mol above the predicted ground state $^4\Sigma^-$ (see Table VII). Thus we would expect that spin-orbit coupling would stabilize the $^4\Phi_{9/2}$ state sufficiently for it to become the ground state. Similarly IrH^+ has the $^4\Phi$ state just 3.8 kcal/mol above the predicted ground state $^4\Sigma^-$. Here again, $^4\Phi_{3/2}$ would be stabilized by spin-orbit coupling, probably becoming the ground state.

For PtH^+ the $^1\Delta$ state is found to be just 1 kcal/mol above the predicted ground state ($^1\Sigma^+$), so that $^3\Delta_1$ will become the ground state after including spin-orbit coupling. In addition, for WH^+ (where $^5\Delta$ is 1.5 kcal/mol higher than the predicted ground state of $^5\Pi$) spin-orbit coupling might change the ground-state symmetry.

Acknowledgment. The calculations and discussions rest heavily on the approaches and conclusions from systematic studies on the first two rows of transition-metal hydrides carried out by Dr. J. B. Schilling (now at Amoco Research Center) in collaboration with Professor J. L. Beauchamp (Caltech) and one of the authors (W.A.G.). The calculations were supported by the National Science Foundation (Grant No. CHE-8318041). One of the authors (G.O.) is grateful to NATO for a fellowship supporting part of his stay at Caltech. In addition, the computer resources (Alliant FX8/8 and DEC VAX 8650) were funded by ONR/DARPA, NSF-MRG, ONR-SRO, and DOE-ECUT.

Molecular Orbital Study on the Mechanism of Oxidation of a Beryllium Atom in Acidic Solution

Kenro Hashimoto,† Nobuyuki Yoda, Yoshihiro Osamura,* and Suehiro Iwata

Contribution from the Department of Chemistry, Faculty of Science and Technology, Keio University, 3-14-1 Hiyoshi, Kohokuku, Yokohama 223, Japan. *Received December 7, 1989*

Abstract: To elucidate the mechanism of metal hydrolysis in acidic solution, we have studied the reaction of a beryllium atom in acidic aqueous solution with ab initio molecular orbital theory. The oxidation process from Be^0 to Be^{II} via Be^I can be regarded as the successive reaction between a Be atom and H_3O^+ ions, assisted by the surrounding water molecules. Although the apparent reacting species are a Be atom and hydronium ions, it is shown that the hydration by water molecules is essential in stabilizing the reacting system at every step. The intermediate species corresponding to Be^I is found to be a solvated protonated beryllium ($[BeH(H_2O)_n]^+$). In the second stage of the oxidation process, the reaction should involve the interaction between the Be^I species and H_3O^+ to produce an H_2 molecule and a hydrated Be^{2+} ion. The molecular interaction to overcome Coulombic repulsion between these two positively charged species is analyzed in terms of electron-population analysis. It is concluded that the large exothermicity due to the hydration of Be^{II} leads to the oxidation of solvated Be^0 and to the production of a hydrogen molecule.

Introduction

A standard textbook of electrochemistry tells us that if the standard reduction potential of a metal is more negative than that of the hydrogen electrode, the metal is oxidized in aqueous solution to produce hydrogen gas. The reaction can be expressed by the following redox equation

$$M + nH^+ + aq \rightarrow M^{n+}aq + (n/2)H_2 \quad (1)$$

which is formally the reaction among a metal, protons, and solvent waters to form a solvated metal ion and molecular hydrogens.[1]

† Present address: Special Researcher, Basic Science Program, The Institute of Physical and Chemical Research (RIKEN), Wako, Saitama 351-01, Japan.

(1) Cotton, F. A.; Willkinson, G. *Advanced Inorganic Chemistry*, 5th ed.; Wiley: New York, 1988; p 97.

0002-7863/90/1512-7189$02.50/0